Title
Arene-Perfluoroarene Interactions in Solution

Journal
The Journal of Organic Chemistry, 86(12)

ISSN
0022-3263

Authors
Lee, Ga Young
Hu, Elizabeth
Rheingold, Arnold L
et al.

Publication Date
2021-06-18

DOI
10.1021/acs.joc.1c00921

Peer reviewed

HHS Public Access

Author manuscript

J Org Chem. Author manuscript; available in PMC 2022 June 18.

Published in final edited form as:

J Org Chem. 2021 June 18; 86(12): 8425–8436. doi:10.1021/acs.joc.1c00921.

Arene-Perfluoroarene Interactions in Solution

Ga Young Lee, **Elizabeth Hu**

Department of Chemistry and Biochemistry, University of California, Los Angeles, California 90095, United States

Arnold L. Rheingold

Department of Chemistry and Biochemistry, University of California, San Diego, California 92093, United States;

K. N. Houk, **Ellen M. Sletten**

Department of Chemistry and Biochemistry, University of California, Los Angeles, California 90095, United States;

Abstract

A systematic study of arene-perfluoroarene interactions in solution is presented. Using a combination of NMR titration experiments, X-ray crystallography, and computational analysis, we analyze the effects of fluorination, substituents, ring size, and solvation on the arene-perfluoroarene interaction. We find that fluorination, extension of the π systems, and enhancement of solvent polarity greatly stabilize the stacking energy up to 3 orders of magnitude (K_a = <1 to 6000 M^{-1}), with the highest K_a achieved for the interaction of water-soluble variants of perfluoronaphthalene and anthracene in buffered D_2O (pD = 12). Combining computational and experimental results, we conclude that this impressive binding energy is a result of enthalpically favorable electrostatic and dispersion interactions as well as the entropically driven hydrophobic effect. The enhanced understanding of arene-perfluoroarene interactions in aqueous solution sets the stage for the implementation of this abiotic intermolecular interaction in biology and medicine.

Graphical Abstract

Corresponding Authors: K. N. Houk – Department of Chemistry and Biochemistry, University of California, Los Angeles, California 90095, United States; houk@chem.ucla.edu, **Ellen M. Sletten –** Department of Chemistry and Biochemistry, University of California, Los Angeles, California 90095, United States; sletten@chem.ucla.edu.

Supporting Information

The Supporting Information is available free of charge at https://pubs.acs.org/doi/10.1021/acs.joc.1c00921.

Equations and error analysis for K_a determination; supporting figures; ^{1}H NMR titration data for all arene-perfluoroarene and arene-arene complexes; crystallographic information for complex **2b·4**, **3b·4**, **1b·5a**, **2b· 5a**, and **3b·5a**; computational results and coordinates; ^{1}H, ^{13}C{1H}, and ^{1}F NMR spectra of compounds **S1**, **1a**, **2a**, **3a**, **3b**, **S2**, **S3**, **5b**, **S4**, and **S5** (PDF)

Accession Codes

CCDC 2060321–2060325 contain the supplementary crystallographic data for this paper. These data can be obtained free of charge via www.ccdc.cam.ac.uk/data_request/cif, or by emailing data_request@ccdc.cam.ac.uk, or by contacting The Cambridge Crystallographic Data Centre, 12 Union Road, Cambridge CB2 1EZ, UK; fax: +44 1223 336033.

Complete contact information is available at: https://pubs.acs.org/10.1021/acs.joc.1c00921

The authors declare no competing financial interest.

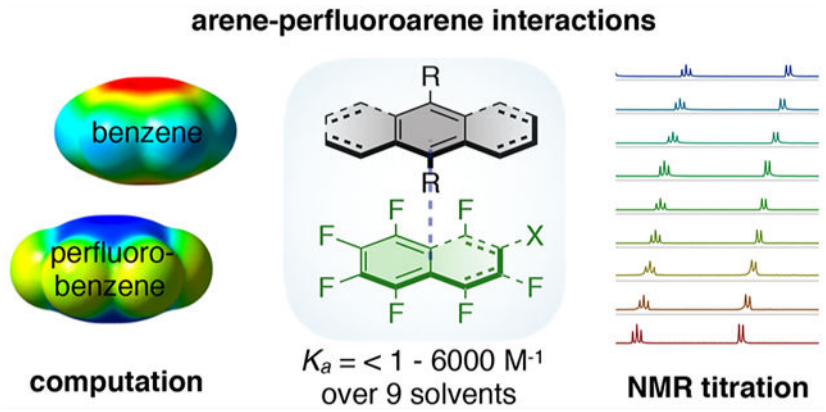

INTRODUCTION

Noncovalent interactions are abundant in both chemical and biological systems and are crucial to molecular recognition, self-assembly, catalysis, and transport.[1–4] When isolated as individual events, noncovalent interactions are quite weak (ΔH = −0.5 – −3 kcal mol^{-1});[5] however, when combined together they result in strong materials, such as Kevlar, or high affinity complexes, such as biotin-(strept)avidin.[6] The ability to engineer noncovalent interactions has led to dynamic materials, sensors, and catalysts, as well as potent therapeutics.[1,7,8]

Among noncovalent interactions, arene-arene interactions, or so-called π–π interactions, are ubiquitous in many molecular organization and recognition processes.[9] Benzene, the simplest arene, is a nonpolar compound with a significant quadrupole moment. Benzene-benzene interactions have two isoenergetic ground state geometries: T-shaped and slip-stacked (Figure 1a).[10] The T-shaped geometry arises from favorable electrostatic interactions between the benzene quadrupoles, while the slip-stacked orientation is dominated by favorable dispersion interactions.[11] Dispersion interactions, atom–atom interactions proportional to distance and polarizability, are increasingly accepted as playing a key role in stabilizing arene-arene interactions.[12–16] Both dispersion and electrostatic interactions contribute to enthalpic stabilization of π–π interactions. When placed in aqueous media, the hydrophobicity of arenes leads to additional stabilization from the hydrophobic effect (Figure S1).

An intriguing and less explored π–π interaction is that between arenes and perfluoroarenes (Figure 1b). The arene-perfluoroarene interaction was first discovered in 1960 when Patrick and Prosser observed that an equimolar mixture of benzene and hexafluorobenzene formed crystals which melt at a higher temperature than crystals from each of the pure components.[17] Aromatic and perfluoroaromatic compounds have opposite quadrupoles, due to the large differences in electronegativity of hydrogen and fluorine atoms (Figure S2). Complementary quadrupoles would favor the sandwich conformation (Figure 1c, left); however, dispersion interactions between polarizable elements, C and H, favor the slip stacked conformation (Figure 1c, middle). Balancing the electrostatic complementarity and dispersion interactions

leads to an overall enthalpically favorable slip stacking interaction as seen in Figure 1b.[11,14,18,19]

Since the initial report of the benzene-hexafluorobenzene cocrystal,[7] applications of arene-perfluoroarene interactions were explored in the solid-state with utility in polymerization[20] and crystal engineering.[21–25] More recently, arene-perfluoroarene interactions have been applied in solution for stabilizing biomolecule-protein interactions and facilitating selective bioconjugation reactions.[26–33] The abiotic nature of perfluoroarenes renders arene-perfluoroarene interactions a promising bioorthogonal noncovalent interaction.[34] Despite this potential, there has not been a systematic study of the aqueous strengths of arene-perfluoroarene interactions experimentally or computationally.

Previously, theoretical studies have predicted a gas phase binding energy for the prototypical benzene-perfluorobenzene interaction (ΔE_{gas} = −5.4 kcal mol^{-1}) that is at least twice as large as the benzene-benzene dimer (ΔE_{gas} = −2.5 kcal mol^{-1}).[11] Several experimental studies verified the binding strengths of the simple arene-perfluoroarene interaction using phenyl and perfluorophenyl moieties in organic solvents (ΔG ~ −1.2 to −1.6 kcal mol^{-1})[35,36] and water (ΔG ~ −1 to −5 kcal mol^{-1}),[27,28,30] where the maximum value is obtained. This collection of data suggests that even the simplest arene-perfluoroarene interaction benefits from the hydrophobic effect (Figure 1c, right). Additionally, these data showcase the potential for arene-perfluoroarene interactions to substitute traditional π–π interactions as molecular synthons. However, many of the previous studies report only on the binding strengths of simple benzene-perfluorobenzene[27,28,30,32,35] and/or use large and complex architectures, making it difficult to decouple the arene-perfluoroarene interaction from other noncovalent interactions occurring within the system.

To obtain a complete understanding of arene-perfluoroarene interactions in solution, we have performed a systematic study of arene-perfluoroarene interactions that includes polycyclic aromatics. We report experimental and computational studies to understand the nature, energetics, and topological characteristics of arene-perfluoroarene interactions (Figure 1c). NMR and X-ray crystallography resulted in binding affinities and optimal geometries of arene-perfluoroarene interactions. Additionally, we employed DFT calculations and energy decomposition analysis to further elucidate the energetic components of arene-perfluoroarene interactions. Using both experimental and computational approaches, we explore the effects of fluorination, substituent, ring size, and solvation on arene-perfluoroarene interactions in organic and aqueous media. The stacking energies are highly dependent on ring size and solvent environment, with K_a's spanning 4 orders of magnitude.

RESULTS

Compound Design and Synthesis.

Accurate experimental and computational measurements of individual noncovalent interactions present many challenges. Supramolecular systems and molecular balances[37–40] are often used to study weak noncovalent interactions; however, these systems are synthetically complex with limited substrate scope and utilize prepositioned binding

geometries. These limitations prevent accurately capturing all thermodynamic parameters of a binding event, particularly the entropic cost of binding. Small molecule systems allow association constants to be measured without constraints; however, this benefit comes at the price of overall low binding free energy due to the inclusion of the large entropic penalty of bimolecular association. When these values are too low (mainly $K_a < 1$), the measurements can be inconclusive due to difficulties in reaching saturation and opportunities for multiple binding modes and geometries.

Considering these limitations, we probed the thermodynamics of arene-perfluoroarene interactions in solution, using small molecules such that we can fully account for solvation and entropy considerations. We synthesized a series of arenes and perfluoroarenes with differing ring sizes and solubilizing groups (Figure 2a,b and Figure S3). We built upon Iverson and co-workers' electron rich tetraethylene glycol-modified naphthalene **2a** as a successful example of an arene appropriate for determination of binding affinities in aqueous and organic media via NMR.[41] We prepared similarly substituted benzene and anthracene compounds (**1a** and **3a**, respectively). The arenes, **1a**, **2a**, and **3a**, were well solubilized in organic and/or aqueous solvents, and we confirmed that the arenes do not self-aggregate by concentration dependent ^{1}H NMR spectra in D_2O (Figure S4). Commercially available perfluoroarenes **4** and **5a** were used as organic-soluble fluoroarenes. Perfluoronaphthalene variant **5b**, containing a methylammonium group, was synthesized and employed as an aqueous-soluble fluoroarene. Attaching ethylene glycol moieties through a benzamide functional group on the fluoroarene did not exhibit sufficient water solubility (Figure S3 compound **S4** and **S5**), and therefore could not be used in the titration study. Compounds **1**–**5** were combined to give six arene-perfluoroarene complexes (Figure 2b) that facilitated the systematic study of the thermodynamics of arene-perfluoroarene interactions.

NMR Titration.

To determine the binding affinities of arene-perfluoroarene interactions, we performed NMR titrations analogous to host–guest binding studies. Arenes were considered "hosts" and kept at a constant, low concentration (0.8 mM) to avoid self-aggregation. Perfluoroarenes were deemed "guests" and their concentration was varied (0–1000 mM). The lack of protons on the perfluoroarenes enabled the chemical shift changes of the aromatic protons on the arenes to be readily analyzed. Each titration experiment involved 10–14 measurements with increasing perfluoroarene concentration until either the solubility limit of the guest or saturation was reached (see SI for further details).

A sample titration experiment between perfluoronaphthalene **5a** and naphthalene **2a** in deuterated methanol is shown in Figure 3a. Significant concentration dependent chemical shift changes were observed only in the aromatic regions, indicative of π–π stacking (Figure S5). All aromatic protons were upfield shifted due to anisotropy of the ring current.[42–44] The largest upfield shifts were observed for the inner aromatic proton H_a, suggesting a strong overlap of the aromatic faces.

Binding stoichiometry was determined by comparing the fitting quality and binding isotherm shapes. Despite the high concentration of perfluoroarene employed in the majority of experiments, our data best matched a 1:1 binding geometry.[45,46] The binding affinities

were determined by inputting the shifts of the aromatic protons into eqs S1, S2, and S3 (see SI) and evaluating their binding isotherms in Igor Pro. In order to unbiasedly determine each K_a value within the experimental limitations, an average of all the aromatic protons was used (Figure 3b) except in the cases when the host protons in the aromatic region overlapped with guest signals and/or had a change of <0.005 ppm. For low binding complexes, we were not able to reach reasonable saturation within the guest solubility limit and the final projected saturation ppm values can be found in the Supporting Information (pages S12–S26).

All data collected can be found in Table 1, with raw NMR data provided as Supporting Information (page S12–S26). Unfortunately, commercial octafluoronaphthalene **5a** contained trace amounts of hydrogenated fluoronaphthalene isomers which were evident at high concentrations (>250 mM) (Figure S6). All attempts at purification were unsuccessful. To ensure that the impurities did not bias the arene-perfluoroarene K_a determinations, we performed an analogous titration for complex **5a·3a** using **5a** with higher impurity content and found no statistically significant difference in K_a values (Figure S7).

Crystallography.

To further elucidate the binding geometries between the arenes and perfluoroarenes employed in this study, we obtained cocrystals (Figure 4). Methyl ether variants of the arenes (**1b**, **2b**, and **3b**) were prepared or purchased (Figure S3) and combined with perfluorobenzene or perfluoronaphthalene. Crystals were obtained by slow evaporation of mixtures of organic solvents at 0 °C. Compounds **1b**, **2b**, and **3b** were utilized in these studies as they were solids at room temperature. We obtained crystal structures for all complexes except **1b**-perfluorobenzene, which was not stable at room temperature. In the five structures obtained, the plane-to-plane distances between aromatic rings are 3.37 to 3.50 Å, which are indicative of a strong π–π interaction.

Computational Analysis.

Using the experimentally determined geometries from the crystallography, we then performed computational energy decomposition analysis (second generation ALMO-EDA)[47] to further unravel the nature of arene-perfluoroarene energetics. The crystal structures represent one of likely many accessible geometries for the weakly bound complexes in solution, but nonetheless, help elucidate the electronic driving forces for the arene-perfluoroarene association. The total interaction energy was decomposed into five components: electrostatic, dispersion, Pauli repulsion, polarization, and charge transfer. We employ these computational results alongside experimental data to gain insight on the effects of fluorination, ring size, and solvation in modulating the strength of arene-perfluoroarene interactions.

DISCUSSION

Fluorination Effects.

First, we experimentally quantified the difference between perfluoroarene-arene and arene-arene binding affinities. We compared binding affinities with perdeutero- and perfluoro-aromatics with anthracene **3a** in CD_3OD. We employed **3a** as the arene due to the fact that it

provided the largest K_a values of the arene partners tested. Despite the K_a values for the interactions of **3a** with both perfluoroaromatics **4** and **5a** in CD_3OD being favorable (K_a = 1.2 M^{-1} and 4.7 M^{-1}, respectively), measurements with deuterated benzene and deuterated naphthalene both yielded $K < 1\ M^{-1}$ a (Figure 5a). From these results, we can conclude that the perfluoroarene-arene interaction is stronger than the arene-arene interaction, with at least a 4-fold increase for naphthyl-anthryl interactions. These results provide direct evidence that arene-perfluoroarene interactions are stronger than arene-arene interactions, as suggested by previous computational and experimental results.[20,41]

We obtained further evidence of the enhanced binding affinity of arenes to perfluoroarenes by comparing naphthyl-naphthyl interactions ($K_a < 1\ M^{-1}$) to naphthyl-perfluoronaphthyl interactions (K_a = 3.5 M^{-1}), where at least a 3-fold difference was observed (Figure 5a). Notably, we also attempted to measure perfluoronaphthalene-perfluoronaphthalene interactions and did not find any detectable association in CD_3OD. This could be due to the limited polarizability of C–F bonds causing reduced dispersion interactions, and high electronegativity of fluorine atoms leading to Coulombic repulsion between Fs in the two molecules. The overall binding strengths of different arenes that have similar surface areas increase in the following order: perfluoroarene-perfluoroarene < arene-arene < arene-perfluoroarene.

To gain a more detailed understanding of the enthalpic effect of fluorination, we employed computational analysis. We took the crystal structure of the naphthyl-naphthyl complex **2a·5a** and computationally performed systematic replacement of fluorine atoms with hydrogen atoms, without altering the geometry (Figure 5b). We employed second generation ALMO-EDA coupled with B97M-V and revPBE functionals, as this method previously has been shown to accurately calculate the interaction energy components of π–π stacking interactions (Figure 5c).[47] ALMO energy decomposition indicates that the interaction between **2b** and **5a** is overall −13.8 kcal mol^{-1} and mainly consists of electrostatic (ΔE_{elec} = −18.3 kcal mol^{-1}) and dispersion interactions (ΔE_{disp} = −18.3 kcal mol^{-1}), which are partly offset by Pauli repulsion (ΔE_{Pauli} = 24.8 kcal mol^{-1}). When all the F atoms in complex **2b·5a** were replaced with H atoms to yield a **2b·$C_{10}H_8$** complex, a large decrease in total interaction energy of 7.6 kcal mol^{-1} (55%) is observed. The ALMO energy decomposition analysis further reveals that Pauli repulsion remains relatively constant, but there are decreases in stabilizing dispersion ($\Delta\Delta E_{disp}$ = 1.6 kcal mol^{-1}) and electrostatic interactions ($\Delta\Delta E_{elec}$ = 4.5 kcal mol^{-1}). This result suggests that the reversal of quadrupole direction is a major factor in stabilizing the arene-perfluoroarene complexes.

Substituent Effects.

The arenes employed in our studies have solubilizing groups, R, attached to the aromatic system. Substituent effects in π–π interactions have long been discussed in the literature[48] and there are currently two main prevailing views: the Hunter–Sanders model[49] and the Houk–Wheeler model.[12] The Hunter–Sanders model, or polar-π model, was first proposed in the early 1990s and suggests that substituents modify the π-electron density, and thereby either enhance or reduce the electrostatic and dispersion interactions with the other arene.[49] The Houk–Wheeler model, the direct interaction model, was proposed in the late 2000s and

suggests that substituents interact directly with the other arene, through electrostatic and dispersion interactions. In the Houk–Wheeler model, the direct substituent interactions are more significant than changes in the π–π interactions of the interacting benzenes.[12] Supported by experimental and computational evidence, the Houk–Wheeler model is now often invoked to understand the energetics of substituent effects in arene-arene interactions.[13,50–53]

In this section, we applied further computational EDA to understand the electronic nature of substituent effects on arene-perfluoroarene interactions. We again performed systematic replacement of atoms in the crystal structure of **2a·5a** (Figure 6a). When the two methoxy groups are substituted with H (complex **$C_{10}H_8$·5a**), the total computed interaction energy decreases by 3.6 kcal mol^{-1} (26%, Figure 6b). The EDA analysis shows that the removal of the methoxy groups leads to similar degrees of reduction in electrostatic and dispersion energy components. Nonetheless, complex **$C_{10}H_8$·5a** still retains a strong interaction (−10.2 kcal mol^{-1}), suggesting that the majority of stabilization is from the simple arene-perfluoroarene binding.

We also performed the reverse subtraction on **2b·5a** where the naphthyl ring of **2b** was removed and the substituents were capped with H atoms to yield two methanol substituents interacting with perfluoronaphthylene (complex **$(MeOH)_2$·5a** in Figure 6a). The interaction between the substituents and octafluoronaphthalene is −4.1 kcal mol^{-1}, which is similar to the difference between **2b·5a** and **$C_{10}H_8$·5a** (−13.8 to −10.2 = −3.6 kcal mol^{-1}). These calculations indicate that the overall interaction energy of **2b·5a** (−13.8 kcal mol^{-1}) results from substituent-π (−4.1 kcal mol^{-1}) and the simple arene-perfluoroarene **$C_{10}D_8$·5a** (−10.2 kcal mol^{-1}) interactions. This finding agrees with Houk and Wheeler's observation that the substituents on the aromatic ring participate in direct interaction with the π system.[12]

In order to further understand the unique planar orientation of **2b·5a**, we found previously reported complexes between other dimethoxy-naphthalene isomers and octafluoronaphthalene, which displayed different planar orientations, and performed similar computational analyses (Figure S8).[54] Upon substituting the two methoxy groups with H for each complex, the resulting simple arene-perfluoroarene complexes display identical interaction energies (−10.0 and −10.2 kcal mol^{-1}). This result suggests that in order to maximize substituent-π interactions, the substituents may induce arene and perfluoroarene rotation around the axis orthogonal to their planes, as long as the slip-stacked orientation can be preserved. In fact, in solution, weakly bound complexes have a shallow potential energy well and populate a number of different arrangements. Overall, the crystal structure data analyzed here indicate that arene-perfluoroarene complexes are most likely to adopt slip-stacking where aromatic rings may rotate in the plane of stacking. Our analysis suggests that substituents linearly augment the binding and alter the mutual orientation of the two π systems, while the interaction between arene and perfluoroarene is likely the major contributor to the overall stacking interaction.

Ring Size Effects.

Next, we analyzed the impact of ring sizes in arene-perfluoroarene interactions by comparing six complexes with differing ring sizes: **1a·4**, **2a·4**, **3a·4**, **1a·5a**, **2a· 5a**, and **3a·5a**

(Figure 7a). We found that increasing the surface area of either the aryl or perfluoroaryl unit increases the binding affinities of the arene-perfluoroarene complexes. As the surface area of contact between the dimers becomes larger than 4 rings, the K_a in CD_3OD surpasses 1.0 kcal mol^{-1} and the Gibb's free energy becomes negative. This suggests that the enthalpy of a relatively simple arene-perfluoroarene interaction can overcome the entropic cost of dimerization. This experiment was repeated in MeCN-d_3 and the same qualitative trend is achieved (Figure S9).[55]

As the size of arenes and perfluoroarenes are increased, the hydrophobicity, polarizability, and quadrupole moment are increased. When analyzing each of these effects on K_a, we must consider their enthalpic and entropic contributions. A molecule's hydrophobicity contributes to the hydrophobic effect in solution, which is mainly entropic at room temperature. In contrast, its polarizability and quadrupole moment impact the dispersion and electrostatic components, respectively, which both contribute to the enthalpy of binding. While we did not directly measure ΔH and ΔS, we utilized computational (this section) and experimental data (solvent effects section) to obtain insights into both thermodynamic parameters.

We first employed ALMO-EDA computational analysis[47] to analyze the enthalpic effects. As seen in Figure 7b, energy values for polarization and charge transfer are calculated to be consistently low for all complexes, indicating that the interaction mainly comes from electrostatic, dispersion, and Pauli repulsion interactions. A plot of the calculated gas phase ΔE_{elec} or ΔE_{disp} values vs the experimental $\Delta G_{MeCN\text{-}d3}$ displays a strong linear correlation with a larger slope for the electrostatic component (Figure 7c). We used experimental K_a values in MeCN-d_3, as these are closer to gas phase binding energies than those measured in CD_3OD. This result suggests that, while electrostatic energy dominates for smaller complexes, dispersion energy dominates for larger complexes. This is probably due to larger complexes having more atom-to-atom contacts, causing enhanced dispersion interactions. In contrast, quadrupole moments of larger arenes are not significantly increased (−29.5 C m^2 for benzene, −44.4 C m^2 for naphthalene, and −61.6 C m^2 for anthracene),[56] therefore decreasing the relative contribution from electrostatic energy. In fact, although these electrostatic and dispersion components are comparable, the differences are quite small. Overall, the trend in ring sizes suggests larger arenes and/or perfluoroarenes should be employed, if possible, to achieve maximum binding affinity.

Solvent Effects.

Finally, we evaluated the contribution of solvation in both organic and aqueous solvents. Through these studies we were able to evaluate the impact of the hydrophobic effect on the binding affinities of arene-perfluoroarene interactions. Initially, we measured the K_a of model complexes **3a·4** and **3a·5a** in a series of readily available deuterated polar organic solvents in which perfluorobenzene **4** and perfluoronaphthalene **5a** are soluble. Figure 8 shows that binding affinities for both complexes increase as solvents change from polar aprotic ($CDCl_3$, CD_3CN, DMSO-d_6) to polar protic (CD_3OD and 3:1 CD_3OD:D_2O).

To continue the series of measurements into aqueous mixtures, we used complex **3a·5b** as a model system where a perfluoronaphthalene containing an ammonium functionality was employed (compound **5b**). Binding affinity measurements with both perfluoronaphthalene

5a and water-soluble perfluoronaphthalene **5b** in 3:1 CD_3OD:D_2O, showed that the addition of the water-solubilizing group did not significantly change the binding affinities (K_a = 21.8 M^{-1}, entry 18 and K_a = 18.9 M^{-1}, entry 19, Table 1). Importantly, these results suggest that the chemical perturbations necessary to achieve water solubility do not introduce significant new intermolecular interactions, particularly a cation-π interaction between the ammonium and the electron-rich aromatic ring. As the percentage of D_2O in CD_3OD is increased from 25% to 100%, there is a 2.6-fold increase in binding affinity. This overall positive trend in K_a from polar aprotic to aqueous media can be attributed to the solvophobicity of minimally polarizable perfluoroarenes, i.e., the hydrophobic effect.[41,57]

Finally, we aimed to quantify how the arene-perfluoroarene interaction is influenced by salts. Pentelute and co-workers discovered that salt accelerates the kinetics of cysteine bioconjugation with the π-clamp, which leverages the arene-perfluoroarene interaction.[58] In our study, addition of a neutral salt (KCl) enhances K_a by 2.4-fold, whereas, more strikingly, addition of the same amount of basic salts (K_2HPO_4 and K_3PO_4, buffered at pD = 12) enhanced the K_a by more than 12-fold. In basic conditions, **5b** is neutral, and the hydrophobicity of the neutral amine is greater than that of the charged ammonium, leading to stronger interactions with **3a**. This result suggests that the arene-perfluoroarene interaction is favored not only by dispersion and electrostatic energy components (enthalpic) but also to a large extent by the hydrophobic effect (entropic) in aqueous environment. Likewise, the arene-perfluoroarene interaction is largely tunable with solvent environment and can be greatly enhanced in aqueous and/or salt environments[37] to reach magnitudes similar to those observed for other host–guest complexes.[6]

CONCLUSIONS

We have performed a systematic and quantitative study of arene-perfluoroarene interactions in solution using a combination of titration, X-ray crystallography, and computational analysis. We quantified arene-perfluoroarene interactions in different media and studied several physical organic phenomena including the effects of fluorination, substituents, ring size, and solvation. We find that fluorination enhances the π–π stacking energy up to 4-fold, by a combination of electrostatic and dispersion energies. Increasing the solvent polarity as well as ionic strength can greatly stabilize the π–π stacking energy up to 4 orders of magnitude. The highest K_a of 6000 M^{-1} was achieved in buffered water (pD = 12), where the large magnitude of this association is attributed to a significant hydrophobic effect. Overall, the collection of experimental and computational data suggests that arene-perfluoroarene interactions are stabilized by both favorable enthalpy (from electrostatic and dispersion interactions) as well as entropy (from the hydrophobic effect) in aqueous solution. These characteristics make the arene-perfluoroarene interaction a promising noncovalent interaction for biological applications.

EXPERIMENTAL SECTION

Materials.

All solvents and reagents were available from commercial sources (Acros Organics, SageChem, Alfa Aesar, Fisher Scientific, Sigma-Aldrich, or TCI) and used without further

purification. Anhydrous and deoxygenated solvents were dispensed from a Grubb's-type Phoenix Solvent Drying System constructed by J.C. Meyer. Flash chromatography was performed using silica gel with 60 Å pores and 40–63 μm mesh particle size (Sorbtech Technologies).

Instrumentation.

^{1}H, ^{19}F, and ^{13}C NMR were taken on Bruker Advance AV-400, AV-500, and DRX-500 and processed with MestReNova or TopSpin software. Chemical shifts are expressed in parts per million (ppm, δ) in reference to residual solvent ($CHCl_3$ at δ = 7.26 ppm or CH_3OH at δ = 3.30 ppm) for compound characterization or to respective solvent signals for titration experiments. Splitting patterns are recorded as singlet (s), doublet (d), triplet (t), quartet (q), pentet (p), multiplet (m), and broad (br). High resolution mass spectra were obtained on Thermo Scientific Q Exactive Plus Hybrid Quadrupole Orbitrap with electrospray ionization (ESI) with Dionex UltiMate 3000 RSLCnano System or Agilent 7250 Q-TOF GC/MS with low energy electroionization (EI).

Binding Affinity Determination.

Binding affinities were determined via inputting the shifts of the aromatic protons into eq S1, S2, and S3 (page S2) and evaluating their binding isotherms in IgorPro. Binding stoichiometry was carefully determined by comparing the fitting quality and binding isotherm shape. To unbiasedly determine a K_a value, an average of all the aromatic protons was used except in the cases when the host protons in the aromatic region overlapped with guest signals and/or had a small change of <0.005 ppm (eq S4 and S5 in page S2). Error ranges are determined within 95% confidence interval (eq S6 in page S2).

Computation.

The geometries of the arene-perfluoroarene complexes were extracted from their corresponding crystal structures. In the study of substituent effects, methoxy substituents, fluorine atoms, and the arene were replaced with H atom at 1.09 Å to yield complex **$C_{10}H_8$·5a**, **2b·$C_{10}H_8$**, and **$(MeOH)_2$·5a**, respectively. Energy decomposition analysis (EDA) for each dimer was performed using second generation (ALMO)-EDA[47] using B97M-V[59] and revPBE3[60] functionals. Additional electronic interaction energies, E_{int}, were calculated using single-point energy calculations at the M06–2*X*/6–311+G(d,p)[61] level of theory. All quantum chemical calculations were performed using Gaussian 09[62] or Q-Chem.[63] All graphics on optimized structures were generated with CYLview.[64]

Synthesis of Functionalized TEG Linker.

Toluene-4-sulfonic acid 2-{2-[2-(2-hydroxy-ethoxy)ethoxy]ethoxy}ethyl ester, S1.—Tetra(ethylene glycol) (150 mL, 779 mol, 10.4 equiv) and THF (30.0 mL) was added to a 500 mL round-bottom flask. Sodium hydroxide (4.80 g, 120 mmol, 1.60 equiv) was dissolved in DI water (30.0 mL) and then added to the reaction flask. The mixture was cooled to 0 °C and *p*-toluensulfonyl chloride (14.3 g, 74.9 mmol, 1.00 equiv) in THF (90 mL) was added slowly over 1 h. The mixture was stirred an additional 2.5 h at 0 °C. Then the mixture was poured into DI water (450 mL), and the layers were separated. The aqueous

phase was extracted with CH_2Cl_2 (4 × 150 mL). The combined organic layer was washed with DI water (3 × 150 mL), dried with $MgSO_4$, and concentrated under reduced pressure. The final compound was yellow oil and used without further purification (24.7 g, 71.2 mmol, 95%). ^{1}H NMR (500 MHz, Chloroform-*d*) δ 7.74 (d, J = 8.6 Hz, 2H), 7.30 (d, J = 8.4 Hz, 2H), 4.11 (t, J = 6.8 Hz, 2H), 3.69–3.49 (comp, 14H), 2.76–2.70 (br s, 1H), 2.39 (s, 3H). ^{13}C{H} NMR (126 MHz, Chloroform-*d*) δ 144.8, 132.9, 129.8, 127.9, 72.5, 70.7, 70.6, 70.4, 70.3, 69.3, 68.6, 21.6. HRMS (ESI) m/z [M + Na]$^+$ calcd for $C_{15}H_{24}O_7SNa$ 371.1140, found 371.1127. ^{1}H NMR matches the literature.[41]

Synthesis of TEGylated Arenes.

2,2′-(((((((1,4-Phenylenebis-(oxy))bis(ethane-2,1-diyl))bis(oxy))bis(ethane-2,1-diyl))bis(oxy))bis-(ethane-2,1-diyl))bis(oxy))bis(ethan-1-ol), 1a.—A 2-neck round-bottom flask was fitted with a reflux condenser, flame-dried in vacuo, and charged with N_2 gas. **S1** (4.00 g, 11.5 mmol, 1.80 equiv) dissolved in anhydrous MeCN (190 mL) was added to the flask. Then hydroquinone (703 mg, 6.4 mmol, 1.00 equiv), potassium carbonate (3.53 g, 25.5 mmol, 3.98 equiv), and lithium bromide (554 mg, 6.4 mmol, 1.00 equiv) were added to the flask. The reaction mixture was allowed to stir at reflux (oil bath) under N_2 atmosphere for 22 h. After cooling, the reaction mixture was filtered and the filter paper was washed with DI H_2O (200 mL). The combined reaction mixture was extracted with DCM (3 × 100 mL), dried with $MgSO_4$, and concentrated under reduced pressure. The crude product was purified via silica gel chromatography, eluting with MeOH/DCM (gradient elution DCM to 5% MeOH/DCM) to afford product **1a** as a faint brown/yellow oil (1.14 g, 2.8 mmol, 43%). ^{1}H NMR (500 MHz, Chloroform-*d*) δ 6.83 (s, 4H), 4.11–4.04 (m, 4H), 3.85–3.79 (m, 4H), 3.75–3.64 (m, 20H), 3.67–3.57 (m, 4H), 2.51–2.43 (s, 2H). ^{13}C{H} NMR (126 MHz, Chloroform-*d*) δ 153.1, 115.6, 72.5, 70.8, 70.7, 70.6, 70.3, 69.9, 68.0, 61.8. HRMS (ESI) m/z [M + Na]$^+$ calcd for $C_{22}H_{38}O_{10}Na$ 485.2362, found 485.2343.

2,2′-(((((((Naphthalene-1,5-diylbis(oxy))bis(ethane-2,1-diyl))bis-(oxy))bis(ethane-2,1-diyl))bis(oxy))bis(ethane-2,1-diyl))bis(oxy))bis-(ethan-1-ol), 2a.—A 2-neck round-bottom flask was fitted with a reflux condenser, flame-dried in vacuo, and charged with N_2 gas. **S1** (2.96 g, 8.50 mmol, 1.81 equiv) was added to the flask using anhydrous MeCN (140 mL). Then 1,5-dihyroxynaphthalene (755 mg, 4.70 mmol, 1.00 equiv), potassium carbonate (2.61 g, 18.9 mmol, 4.02 equiv), and lithium bromide (735 mg, 8.50 mmol, 1.81 equiv) were added to the flask. The reaction mixture was allowed to stir at reflux (oil bath) under N_2 atmosphere for 22 h. After cooling, the reaction mixture was filtered and the filter paper was washed with DI H_2O (170 mL). The combined reaction mixture was extracted with DCM (3 × 70 mL), washed with 3:1 brine:10% NaOH (3 × 70.0 mL), dried with $MgSO_4$, and concentrated under reduced pressure. The crude product was purified via silica gel chromatography, eluting with MeOH/DCM (gradient elution DCM to 5% MeOH/DCM) to afford product **2a** as a faint dark purple oil (1.50 g, 3.24 mmol, 69%). ^{1}H NMR (500 MHz, Chloroform-*d*) δ 7.85 (d, J = 8.5 Hz, 2H), 7.34 (dd, J = 8.4, 7.6 Hz, 2H), 6.84 (d, J = 7.7 Hz, 2H), 4.32–4.26 (m, 4H), 3.99 (dd, J = 5.6, 4.2 Hz, 4H), 3.83–3.77 (m, 4H), 3.73–3.62 (comp, 16H), 3.60–3.55 (m, 4H), 2.49 (td, J = 6.3, 2.8 Hz, 2H). ^{13}C{H} NMR (126 MHz, Chloroform-*d*) δ 154.3, 126.8, 125.1, 114.6, 105.7, 72.5, 71.0, 70.7, 70.3,

69.8, 67.9, 61.8. HRMS (ESI) *m*/*z* [M + Na]$^+$ calcd for $C_{26}H_{40}O_{10}Na$ 535.2519, found 535.2501. ^{1}H NMR matches the literature.[41]

2,2′-(((((((Anthracene-9,10-diylbis(oxy))bis(ethane-2,1-diyl))bis-(oxy))bis(ethane-2,1-diyl))bis(oxy))bis(ethane-2,1-diyl))bis(oxy))bis-(ethan-1-ol), 3a.—A 500 mL 3-neck round-bottom flask was flame-dried in vacuo and charged with N_2 gas. 9,10-anthraquinone (937 mg, 4.50 mmol, 1.00 equiv), tetrabutyl ammonium chloride (101 mg, 0.32 mmol, 0.07 equiv), and sodium dithionite (9.40 g, 54.0 mmol, 12.0 equiv) were added to the flask using THF (180 mL) and DI H_2O (60 mL). Then the flask was freeze–pump–thawed 3 times to remove any dissolved gas. The reaction mixture was stirred for 15 min at room temperature. Then, excess potassium carbonate (10.6 g, 189 mmol, 42.0 equiv) dissolved in DI H_2O (10.0 mL) was added to the reaction flask and stirred for 15 min. Then, **S1** (15.7 g, 45.0 mmol, 10.0 equiv) dissolved in THF (10.0 mL) was added to the reaction flask. The mixture was heated to 50 °C (oil bath) and stirred under N_2 atmosphere for 24h. After cooling, THF was removed. The remaining aqueous mixture was extracted with DCM (3 × 200 mL), dried with $MgSO_4$, and concentrated under reduced pressure. The crude product was purified via silica gel chromatography twice, each time eluting with MeOH/DCM (gradient elution DCM to 5% MeOH/DCM) to afford product **3a** as a faint yellow/green oil (1.49 g, 2.66 mmol, 59%). ^{1}H NMR (500 MHz, Chloroform-*d*) *δ* 8.41–8.34 (m, 4H), 7.50–7.44 (m, 4H), 4.39–4.32 (m, 4H), 4.02–3.97 (m, 4H), 3.87–3.59 (m, 24H), 2.44 (s, 2H). ^{13}C{H} NMR (126 MHz, Chloroform-*d*) *δ* 147.1, 125.3, 125.1, 122.7, 74.8, 72.5, 71.0, 70.8, 70.8, 70.7, 70.4, 61.8. HR-LC/MS (EI) *m*/*z* [M + Na]$^+$ calcd for $C_{30}H_{42}O_{10}Na$ 585.2677, found 585.2723.

Synthesis of Methylated Arene.

9,10-Dimethoxyanthracene, 3b.—A 500 mL 3-neck round-bottom was flask flame-dried in vacuo and charged with N_2 gas. 9,10-Anthraquinone (1.46 g, 7.00 mmol, 1.00 equiv), tetrabutyl ammonium chloride (158 mg, 0.49 mmol, 0.07 equiv), and sodium dithionite (14.6 g, 84.0 mmol, 12.0 equiv) were added to the flask using THF (200 mL) and DI H_2O (50 mL). Then the flask was freeze–pump–thawed 3 times to remove any dissolved gas. Reaction mixture was stirred for 15 min at room temperature. Then, excess potassium carbonate (16.5 g, 294 mmol, 42.0 equiv) dissolved in DI H_2O (20.0 mL) was added to the reaction flask and stirred for 15 min. Then, methyl iodide (4.36 mL, 20.0 mmol, 2.86 equiv) and extra THF (30.0 mL) were added to the reaction flask. The mixture was heated to 50 °C (oil bath) and stirred under N_2 atmosphere for 24 h. After cooling, THF was removed. The remaining aqueous mixture was extracted with DCM (3 × 200 mL), dried with $MgSO_4$, and concentrated under reduced pressure. The crude product was purified via silica gel chromatograph, eluting with MeOH/DCM (gradient elution DCM to 5% MeOH/DCM) to afford product **3b** as yellow crystals (1.36 g, 3.99 mmol, 57%). ^{1}H NMR (500 MHz, Chloroform-*d*) *δ* 8.34–8.26 (m, 4H), 7.53–7.46 (m, 4H), 4.12 (s, 6H). ^{13}C{H} NMR (126 MHz, Chloroform-*d*) *δ* 148.4, 125.3, 124.9, 122.6, 63.2. HR-GC/MS (EI) *m*/*z* [M]$^+$ calcd for $C_{16}H_{14}O_2$ 238.0994, found 238.0990.

Synthesis of H_2O-Soluble Perfluoroarene.

1,2,3,4,5,6,8-Heptafluoro-7-(nitromethyl)naphthalene, S2.—A 50 mL 2-neck round-bottom flask was flame-dried in vacuo and charged with N_2 gas. Nitromethane (4.90 mL, 110 mmol, 12.0 equiv) and 1,8-diazabicyclo[5.4.0]undec-7-ene (2.90 mL, 19.3 mmol, 2.10 equiv) were added to the flask. Then the mixture was cooled to 0 °C and stirred for 20 min. Octafluoronaphthlene was added in 3 aliquots (total 2.50 g, 9.17 mmol, 1.00 equiv) over 20 min. Then the reaction mixture was stirred 0 °C for another 3 h. The reaction was quenched with 1 M HCl solution saturated with NaCl (30.0 mL, ~2.3 equiv), extracted with EtOAc (3 × 100 mL), dried with $MgSO_4$, and concentrated under reduced pressure. The crude product was purified via silica gel chromatography, eluting with EtOAc/hexanes (gradient elution hexanes to 10% EtOAc/hexanes) to afford product **S2** as a faint yellow solid (1.45 g, 4.59 mmol, 50%). ^{1}H NMR (500 MHz, Chloroform-*d*) δ 5.75 (s, 2H). ^{13}C{H} NMR (126 MHz, Chloroform-*d*) δ 151.9 (d, J = 263.5 Hz, 1C), 145.6 (dd, J = 254.1, 14.0 Hz, 1C), 143.0–137.8 (m, 4C), 113.0–107.6 (m, 1C), 107.2 (s, 1C), 65.9 (s, 2C). ^{19}F NMR (376 MHz, Chloroform-*d*) δ −118.04 to −118.81 (m, 1F), −138.22 (ddt, J = 16.5, 8.0, 4.1 Hz, 1F), −142.47 (dtt, J = 67.8, 16.6, 4.6 Hz, 1F), −144.7 to −145.0 (m, 1F), −147.0 to −147.4 (m, 1F), −150.1 (dddd, J = 22.2, 17.1, 8.6, 4.3 Hz, 1F), −153.7 (dddd, J = 25.7, 18.0, 7.5, 3.8 Hz, 1F). HR-GC/MS (EI) m/z $[M]^+$ calcd for $C_{11}H_2F_7NO_2$ 312.9974, found 312.9969. ^{1}H NMR and ^{19}F-NMR match the literature.[65]

tert-Butyl ((perfluoronaphthalen-2-yl)methyl)carbamate, S3.—A 100 mL 2-neck round-bottom flask was fitted with a reflux condenser and a vent needle. To the flask, Fe powder (892 mg, 16.0 mmol, 5.00 equiv), **S2** (1.00 g, 3.20 mmol, 1.00 equiv), and AcOH (17.0 mL). The reaction mixture was heated to 50 °C (oil bath) and stirred for 24 h. After cooling, AcOH was removed under vacuum. Then triethylamine (4.40 mL, 32.0 mmol, 10.0 equiv), Di-*tert*-butyl decarbonate (1.83 mL, 8.00 mmol, 2.50 equiv), and anhydrous DCM (25.0 mL) were added. The reaction mixture was stirred at room temperature for 24 h. Then solvent was removed under vacuum and the crude product was purified via silica gel chromatography, eluting with EtOAc/hexanes (gradient elution hexanes to 20% EtOAc/hexanes) to afford product **S3** as a faint brown solid (730 mg, 1.92 mmol, 60%). ^{1}H NMR (500 MHz, Chloroform-*d*) δ 5.04 (s, 1H), 4.58 (s, 2H), 1.42 (s, 9H). 13C{H} NMR (126 MHz, Chloroform-*d*) δ 155.2 (s, 1C), 150.6 (d, J = 258.3 Hz, 1C), 146.4 (d, J = 252.6 Hz, 1C), 142.5–137.5 (m, 4C), 116.4–111.0 (m, 1C) 107.9 (s, 1C), 32.9 (s, 2C), 28.3 (s, 9C). ^{19}F NMR (376 MHz, Chloroform-*d*) δ −121.43 (s, 1F), −138.63 (s, 1F), −143.72 (s, 1F), −146.09 (s, 1F), −148.77 (s, 1F), −153.23 (s, 1F), −155.52 (s, 1F). HR-GC/MS (EI) m/z [M – *tert*-butyl(C_4H_8)]$^+$ calcd for $C_{12}H_4F_7NO_2$ 327.0130, found 327.0128.

(Perfluoronaphthalen-2-yl)methanaminium 2,2,2-trifluoroace-tate, 5b.—S3 (361 mg, 0.94 mmol, 1.00 equiv), trifluoroacetic acid (7.20 mL, 94 mmol, 100 equiv), and DCM (36.0 mL) were added to a 100 mL round-bottom flask. The reaction mixture was stirred at room temperature for 20 h. Then solvent was evaporated in vacuo to yield the final product as a light brown powder (290 mg, 0.72 mmol, 77%). The final product was used without further purification. ^{1}H NMR (500 MHz, Methanol-d_4) δ 4.44 (s, 2H). ^{13}C{H} NMR (126 MHz, Methanol-d_4) δ 161.7 (s, 1C), 151.6 (d, J = 260.2 Hz, 1C), 145.8 (d, J = 256.0 Hz, 1C), 142.9–137.6 (m, 4C), 112.1 (s, 1C), 110.5 (t, J = 19.3 Hz, 1C), 107.8 (t, J = 13.7 Hz,

1C), 30.5 (m, 1C). ^{19}F NMR (376 MHz, Methanol-d_4) δ −77.04 (3F), −120.63 (1F), −140.63 (1F), −146.11 (1F), −148.49 (1F), −150.81 (1F), −154.99 (1F), −158.01 (1F). HRMS (ESI) m/z [M – TFA]$^+$ calcd for $C_{11}H_5F_7N$ 284.0310, found 284.0296.

Synthesis of H_2O-Insoluble Perfluoroarenes.

2,3,4,5,6-Pentafluoro-N-(2-hydroxyethyl)benzamide, S4.—A 20.0 mL scintillation vial was oven-dried overnight. Pentafluorobenzoic acid (200 mg, 0.94 mmol, 1.00 equiv), and thionyl chloride (790 μL, 10.9 mmol, 11.6 equiv) were added to the vial. The reaction mixture stirred at reflux for 22 h. After cooling, excess thionyl chloride was removed in vacuo quickly. Ethanol amine (44.3 mg, 0.73 mmol, 0.777 equiv), triethyl amine (131 μL, 0.73 mmol 0.777 equiv), and anhydrous DCM (5 mL) were added to the scintillation vial containing the acid chloride intermediate. The reaction mixture was stirred at room temperature for 12 h. To the reaction mixture was added DI H_2O (10.0 mL), then extracted in DCM (3 × 15.0 mL), dried with $MgSO_4$, and concentrated under reduced pressure. The crude product was purified via silica gel chromatography, eluting with MeOH/DCM (gradient elution DCM to 5% MeOH/DCM) to afford final product **S4** as white powder (146 mg, 0.56 mmol, 60%). ^{1}H NMR (500 MHz, Chloroform-d) δ 6.37 (s, 1H), 3.86 (q, J = 5.0 Hz, 2H), 3.65 (q, J = 5.3 Hz, 2H), 1.81 (s, 1H). ^{13}C{H} NMR (126 MHz, Methanol-d_4) δ 158.4 (1C), 144.9–140.6 (m, 2C), 138.8–136.2 (m, 1C), 112.3 (d, J = 20.2 Hz, 1C), 59.8 (1C), 42.2 (1C). 19F NMR (376 MHz, Chloroform-d) δ −140.19 to −140.34 (m, 2F), −150.22 to −150.41 (m, 1F), −159.72 to −159.92 (m, 2F). HRMS (ESI) m/z [M – H_2O]$^+$ calcd for $C_9H_4F_5NO$ 237.0213, found 237.0206.

2,3,5,6-Tetrafluoro-N1,N4-bis(2-(2-(2-(2-hydroxyethoxy)ethoxy)-ethoxy)ethyl)terephthalamide, S5.—A 100 mL 2-neck round-bottom flask was flame-dried in vacuo and charged with N_2 gas. Tetrafluoroterephthalic acid (200 mg, 0.840 mmol, 1.00 equiv), EDC·HCl (564 mg, 2.94 mmol, 3.50 equiv), HOBt hydrate (397 mg, 2.94 mmol, 3.50 equiv), and anhydrous DCM (20.0 mL) were added to the flask. The reaction mixture was stirred at room temperature under N_2 atmosphere for 1 h. Then 2-(2-(2-(2-aminoethoxy)ethoxy)-ethoxy)ethan-1-ol (974 mg, 5.04 mmol, 6.00 equiv) and triethylamine (1.20 mL, 8.40 mmol, 10.0 equiv) were added to the flask using dry DCM (14.0 mL). The reaction mixture was stirred at room temperature under N_2 atmosphere for additional 20 h. Then the reaction mixture was concentrated in vacuo and the crude product was purified via silica gel chromatography eluting with MeOH/DCM (gradient elution DCM to 4% MeOH/DCM) to afford product **S5** as a faint yellow oil (248 g, 0.420 mmol, 50%). ^{1}H NMR (500 MHz, Chloroform-d) δ 8.46–8.41 (s, 1H), 3.96–3.40 (m, 16H). ^{13}C{H} NMR (126 MHz, Chloroform-d) δ 158.2, 143.1 (d, J = 252.2 Hz), 117.9, 72.4, 70.6, 70.3, 70.2, 69.9, 69.6, 61.1, 39.9. ^{19}F NMR (376 MHz, Chloroform-d) δ −140.98 (s, 4F). HRMS (ESI) m/z calcd for [M + H]$^+$ $C_{24}H_{37}F_4N_2O_{10}$ 589.2384, found 589.2379.

Supplementary Material

Refer to Web version on PubMed Central for supplementary material.

ACKNOWLEDGMENTS

We thank Monica Pengshung, Irene Lim, and Margeaux Miller for helpful discussions. This work was funded by the National Institute of Health (1DP2GM132680 to E.M.S.) and the National Science Foundation (CHE-1764328 to K.N.H.)

REFERENCES

(1). Riley KE; Hobza P Noncovalent Interactions in Biochemistry. Wiley Interdiscip. Rev.: Comput. Mol. Sci 2011, 1 (1), 3–17.

(2). Hobza P;Šponer J Structure, Energetics, and Dynamics of the Nucleic Acid Base Pairs: Nonempirical Ab Initio Calculations. Chem. Rev 1999, 99 (11), 3247–3276. [PubMed: 11749516]

(3). Jurečka P; Hobza P True Stabilization Energies for the Optimal Planar Hydrogen-Bonded and Stacked Structures of Guanine···Cytosine, Adenine···Thymine, and Their 9- and 1-Methyl Derivatives: Complete Basis Set Calculations at the MP2 and CCSD(T) Levels and Comparison with Experiment. J. Am. Chem. Soc 2003, 125 (50), 15608–15613. [PubMed: 14664608]

(4). Salonen LM; Ellermann M; Diederich F Aromatic Rings in Chemical and Biological Recognition: Energetics and Structures. Angew. Chem., Int. Ed 2011, 50 (21), 4808–4842.

(5). Müller-Dethlefs K; Hobza P Noncovalent Interactions: A Challenge for Experiment and Theory. Chem. Rev 2000, 100 (1), 143–167. [PubMed: 11749236]

(6). Houk KN; Leach AG; Kim SP; Zhang X Binding Affinities of Host-Guest, Protein-Ligand, and Protein-Transition-State Complexes. Angew. Chem., Int. Ed 2003, 42, 4872–4897.

(7). Meyer EA; Castellano RK; Diederich F Interactions with Aromatic Rings in Chemical and Biological Recognition. Angew. Chem., Int. Ed 2003, 42, 1210–1250.

(8). Salonen LM; Ellermann M; Diederich F Aromatic Rings in Chemical and Biological Recognition: Energetics and Structures. Angew. Chem., Int. Ed 2011, 50 (21), 4808–4842.

(9). Hwang JW; Li P; Shimizu KD Synergy between Experimental and Computational Studies of Aromatic Stacking Interactions. Org. Biomol. Chem 2017, 15 (7), 1554–1564. [PubMed: 27878156]

(10). Tsuzuki S; Honda K; Uchimaru T; Mikami M; Tanabe K Origin of Attraction and Directionality of the π/π Interaction: Model Chemistry Calculations of Benzene Dimer Interaction. J. Am. Chem. Soc 2002, 124 (1), 104–112. [PubMed: 11772067]

(11). Tsuzuki S; Uchimaru T; Mikami M Intermolecular Interaction between Hexafluorobenzene and Benzene: Ab Initio Calculations Including CCSD(T) Level Electron Correlation Correction. J. Phys. Chem. A 2006, 110 (5), 2027–2033. [PubMed: 16451038]

(12). Wheeler SE; Houk KN Substituent Effects in the Benzene Dimer Are Due to Direct Interactions of the Substituents with the Unsubstituted Benzene. J. Am. Chem. Soc 2008, 130 (33), 10854–10855. [PubMed: 18652453]

(13). Sinnokrot MO; Sherrill D Substituent Effects in π-π Interactions: Sandwich and T-Shaped Configurations. J. Am. Chem. Soc 2004, 126 (24), 7690–7697. [PubMed: 15198617]

(14). Carter-Fenk K; Herbert JM Electrostatics Does Not Dictate the Slip-Stacked Arrangement of Aromatic π-π Interactions. Chem. Sci 2020, 11 (26), 6758–6765. [PubMed: 34094127]

(15). Martinez CR; Iverson BL Rethinking the Term “Pi-Stacking. Chem. Sci 2012, 3, 2191–2201.

(16). Yang L; Brazier JB; Hubbard TA; Rogers DM; Cockroft SL Can Dispersion Forces Govern Aromatic Stacking in an Organic Solvent? Angew. Chem., Int. Ed 2016, 55 (3), 912–916.

(17). Patrick CR; Prosser GS A Molecular Complex of Benzene and Hexafluorobenzene. Nature 1960, 187 (4742), 1021.

(18). Hunter CA; Lawson KR; Perkins J; Urch CJ Aromatic Interactions. J. Chem. Soc., Perkin Trans 2 2001, 651–669.

(19). Hernández-Trujillo J; Costas M; Vela A Quadrupole Interactions in Pure Non-Dipolar Fluorinated or Methylated Benzenes and Their Binary Mixtures. J. Chem. Soc., Faraday Trans 1993, 89 (14), 2441–2443.

(20). Coates GW; Dunn AR; Henling LM; Dougherty DA; Grubbs RH Phenyl-Perfluorophenyl Stacking Interactions: A New Strategy for Supermolecule Construction. Angew. Chem., Int. Ed. Engl 1997, 36 (3), 248–251.

(21). Ponzini F; Zagha R; Hardcastle K; Siegel JS Phenyl/Pentafluorophenyl Interactions and the Generation of Ordered Mixed Crystals: Sym-Triphenethynylbenzene and Sym-Tris-(Perfluorophenethynyl)Benzene. Angew. Chem., Int. Ed 2000, 39 (13), 2323–2325.

(22). Watt SW; Dai C; Scott AJ; Burke JM; Thomas RL; Collings JC; Viney C; Clegg W; Marder TB Structure and Phase Behavior of a 2:1 Complex between Arene- and Fluoroarene-Based Conjugated Rigid Rods. Angew. Chem., Int. Ed 2004, 43 (23), 3061–3063.

(23). Rasmusson T; Martyn LJP; Chen G; Lough A; Oh M; Yudin AK Aromatic Fluorine as a Versatile Control Element for the Construction of Molecules with Helical Chirality. Angew. Chem., Int. Ed 2008, 47 (37), 7009–7012.

(24). Xu R; Schweizer WB; Frauenrath H Soluble Poly-(Diacetylene)s Using the Perfluorophenyl-Phenyl Motif as a Supramolecular Synthon. J. Am. Chem. Soc 2008, 130 (34), 11437–11445. [PubMed: 18652461]

(25). Pawle RH; Haas TE; Müller P; Thomas SW Twisting and Piezochromism of Phenylene-Ethynylenes with Aromatic Interactions between Side Chains and Main Chains. Chem. Sci 2014, 5 (11), 4184–4188.

(26). Cejas MA; Kinney WA; Chen C; Leo GC; Tounge BA; Vinter JG; Joshi PP; Maryanoff BE Collagen-Related Peptides: Self-Assembly of Short, Single Strands into a Functional Biomaterial of Micrometer Scale. J. Am. Chem. Soc 2007, 129 (8), 2202–2203. [PubMed: 17269769]

(27). Zheng H; Gao J Highly Specific Heterodimerization Mediated by Quadrupole Interactions. Angew. Chem., Int. Ed 2010, 49 (46), 8635–8639.

(28). Pace CJ; Zheng H; Mylvaganam R; Kim D; Gao J Stacked Fluoroaromatics as Supramolecular Synthons for Programming Protein Dimerization Specificity. Angew. Chem., Int. Ed 2012, 51 (1), 103–107.

(29). Zhang C; Welborn M; Zhu T; Yang NJ; Santos MS; Van Voorhis T; Pentelute BL π-Clamp-Mediated Cysteine Conjugation. Nat. Chem 2016, 8 (2), 120–128. [PubMed: 26791894]

(30). Woll MG; Hadley EB; Mecozzi S; Gellman SH Stabilizing and Destabilizing Effects of Phenylalanine f F 5-Phenylalanine Mutations on the Folding of a Small Protein. J. Am. Chem. Soc 2006, 128, 15932–15933. [PubMed: 17165695]

(31). Gorske BC; Blackwell HE Tuning Peptoid Secondary Structure with Pentafluoroaromatic Functionality: A New Design Paradigm for the Construction of Discretely Folded Peptoid Structures. J. Am. Chem. Soc 2006, 128 (44), 14378–14387. [PubMed: 17076512]

(32). Lai JS; Qu J; Kool ET Fluorinated DNA Bases as Probes of Electrostatic Effects in DNA Base Stacking. Angew. Chem., Int. Ed 2003, 42 (48), 5973–5977.

(33). Zahn A; Brotschi C; Leumann CJ Pentafluorophenyl-Phenyl Interactions in Biphenyl-DNA. Chem. - Eur. J 2005, 11 (7), 2125–2129. [PubMed: 15714531]

(34). Yoder NC; Yüksel D; Dafik L; Kumar K Bioorthogonal Noncovalent Chemistry: Fluorous Phases in Chemical Biology. Curr. Opin. Chem. Biol 2006, 10, 576–583. [PubMed: 17055332]

(35). Laatikainen R; Ratilainen J; Sebastian R; Santa H NMR Study of Aromatic-Aromatic Interactions for Benzene and Some Other Fundamental Aromatic Systems Using Alignment of Aromatics in Strong Magnetic Field. J. Am. Chem. Soc 1995, 117 (44), 11006–11010.

(36). Adams H; Jimenez Blanco JL; Chessari G; Hunter CA; Low CMR; Sanderson JM; Vinter JG Quantitative Determination of Intermolecular Interactions with Fluorinated Aromatic Rings. Chem. - Eur. J 2001, 7 (16), 3494–3503. [PubMed: 11560319]

(37). Huang Z; Chen X; Wu G; Metrangolo P; Whitaker D; McCune JA; Scherman OA Host-Enhanced Phenyl-Perfluorophenyl Polar-ΠInteractions. J. Am. Chem. Soc 2020, 142 (16), 7356–7361. [PubMed: 32248683]

(38). Faraoni R; Castellano RK; Gramlich V; Diederich F H-Bonded Complexes of Adenine with Rebek Imide Receptors Are Stabilised by Cation-π Interactions and Destabilised by Stacking with Perfluoroaromatics. Chem. Commun 2004, 370–371.

(39). Korenaga T; Kawauchi Y; Kosaki T; Ema T; Sakai T Synthesis of a Molecular Tweezer Containing Pentafluorophenyl Groups and Investigation of The-Stacking Interaction for a Pentafluorophenyl Group in a Polar Organic Solvent. Bull. Chem. Soc. Jpn 2005, 78, 2175–2179.

(40). Gung BW; Xue X; Zou Y Enthalpy (ΔH) and Entropy (ΔS) for π-Stacking Interactions in Near-Sandwich Configurations: Relative Importance of Electrostatic, Dispersive, and Charge-Transfer Effects. J. Org. Chem 2007, 72 (7), 2469–2475. [PubMed: 17338571]

(41). Cubberley MS; Iverson BL 1H NMR Investigation of Solvent Effects in Aromatic Stacking Interactions. J. Am. Chem. Soc 2001, 123 (31), 7560–7563. [PubMed: 11480976]

(42). Riwar L-J; Trapp N; Kuhn B; Diederich F Substituent Effects in Parallel-Displaced π-π Stacking Interactions: Distance Matters. Angew. Chem., Int. Ed 2017, 56 (37), 11252–11257.

(43). Nandy R; Subramoni M; Varghese B; Sankararaman S Intramolecular π-Stacking Interaction in a Rigid Molecular Hinge Substituted with 1-(Pyrenylethynyl) Units. J. Org. Chem 2007, 72 (3), 938–944. [PubMed: 17253814]

(44). Waelès P; Fournel-Marotte K; Coutrot F Distinguishing Two Ammonium and Triazolium Sites of Interaction in a Three-Station [2]Rotaxane Molecular Shuttle. Chem. - Eur. J 2017, 23 (48), 11529–11539. [PubMed: 28594431]

(45). Thordarson P Binding Constants and Their Measurement. Supramol. Chem 2012, DOI: 10.1002/9780470661345.smc018.

(46). Thordarson P Determining Association Constants from Titration Experiments in Supramolecular Chemistry. Chem. Soc. Rev 2011, 40 (3), 1305–1323. [PubMed: 21125111]

(47). Horn PR; Mao Y; Head-Gordon M Probing Non-Covalent Interactions with a Second Generation Energy Decomposition Analysis Using Absolutely Localized Molecular Orbitals. Phys. Chem. Chem. Phys 2016, 18, 23067–23079. [PubMed: 27492057]

(48). Riwar LJ; Trapp N; Kuhn B; Diederich F Substituent Effects in Parallel-Displaced π-π Stacking Interactions: Distance Matters. Angew. Chem., Int. Ed 2017, 56 (37), 11252–11257.

(49). Hunter CA; Sanders JKM The Nature of π-π Interactions. J. Am. Chem. Soc 1990, 112 (14), 5525–5534.

(50). Sinnokrot MO; Sherrill CD Unexpected Substituent Effects in Face-to-Face π-Stacking Interactions. J. Phys. Chem. A 2003, 107 (41), 8377–8379.

(51). Ringer AL; Sinnokrot MO; Lively RP; Sherrill CD The Effect of Multiple Substituents on Sandwich and T-Shaped π-π Interactions. Chem. - Eur. J 2006, 12 (14), 3821–3828. [PubMed: 16514687]

(52). Lee EC; Kim D; Jurečka P; Tarakeshwar P; Hobza P; Kim KS Understanding of Assembly Phenomena by Aromatic-Aromatic Interactions: Benzene Dimer and the Substituted Systems. J. Phys. Chem. A 2007, 111 (18), 3446–3457. [PubMed: 17429954]

(53). Grimme S; Antony J; Schwabe T; Mück-Lichtenfeld C Density Functional Theory with Dispersion Corrections for Supramolecular Structures, Aggregates, and Complexes of (Bio)Organic Molecules. Org. Biomol. Chem 2007, 5 (5), 741–758. [PubMed: 17315059]

(54). Hori A; Takeda H; Premkumar JR; Sastry GN 1:1 and 2:1 Cocrystallizations of Alkoxy-Substituted Naphthalene Derivatives with Octafluoronaphthalene through Arene-Perfluoroarene Interactions. J. Fluorine Chem 2014, 168, 193–197.

(55). We note that the association between benzene and perfluorobenzene (**1a·4**) is not favorable in both the acetonitrile and methanol solutions used in our study. This result is in contrast to the previous findings that report phenyl-perfluorophenyl association Δ*G*. Refer to refs 35 and 36.

(56). Chablo A; Cruickshank DWJ; Hinchliffe A; Munn RW Quadrupole Moment Calculations for Some Aromatic Hydrocarbons. Chem. Phys. Lett 1981, 78 (3), 424–428.

(57). Yang L; Adam C; Cockroft SL Quantifying Solvophobic Effects in Nonpolar Cohesive Interactions. J. Am. Chem. Soc 2015, 137 (32), 10084–10087. [PubMed: 26159869]

(58). Dai P; Zhang C; Welborn M; Shepherd JJ; Zhu T; Van Voorhis T; Pentelute BL Salt Effect Accelerates Site-Selective Cysteine Bioconjugation. ACS Cent. Sci 2016, 2 (9), 637–646. [PubMed: 27725962]

(59). Mardirossian N; Head-Gordon M Mapping the Genome of Meta-Generalized Gradient Approximation Density Functionals: The Search for B97M-V. J. Chem. Phys 2015, 142 (7), 74111.

(60). Zhang Y; Yang W Comment on "Generalized Gradient Approximation Made Simple. Phys. Rev. Lett 1998, 80, 890.

(61). Zhao Y; Truhlar DG The M06 Suite of Density Functionals for Main Group Thermochemistry, Thermochemical Kinetics, Noncovalent Interactions, Excited States, and Transition Elements: Two New Functionals and Systematic Testing of Four M06-Class Functionals and 12 Other Functionals. Theor. Chem. Acc 2008, 120 (1–3), 215–241.

(62). Frisch MJ; Trucks GW; Schlegel HB; Scuseria GE; Robb MA; Cheeseman JR; Scalmani G; Barone V; Petersson GA; Nakatsuji H; Caricato M; Marenich A; Bloino J; Janesko BG; Gomperts R; Mennucci B; Hratchian HP; Ortiz JV; Izmaylov AF; Sonnenberg JL; Williams-Young D; Ding F; Lipparini F; Egidi F; Going J; Peng B; Petrone A; Henderson T; Ranasinghe D; Zakrzewski VG; Gao J; Rega N; Zheng G; Liang W; Hada M; Ehara M; Toyota K; Fukada R; Hasegawa J; Ishida M; Nakajima T; Honda Y; Kitao O; Nakai H; Vreven T; Throssell K; Montgomery A Jr.; Peralta JE; Ogliaro F; Bearpark M; Heyd JJ; Brothers E; Kudin KN; Staroverov VN; Keith T; Kobayashi R; Normand J; Raghavachari K; Rendell A; Burant JC; Iyengar SS; Tomasi J; Cossi M; Milliam JM; Klene M; Adamo C; Cammi R; Ochterski JW; Martin RL; Morokuma K; Farkas O; Foresman JB; Fox DJ Gaussian 09; Gaussian, Inc.: Wallingford, CT, 2013.

(63). Shao Y; Shao Y; Gan Z; Epifanovsky E; Gilbert ATB; Wormit M; Kussmann J; Lange AW; Behn A; Deng J; Feng X; Ghosh D; Goldey M; Horn PR; Jacobson LD; Kaliman I; Khaliullin RZ; Kús T; Landau A; Liu J; Proynov EI; Rhee YM; Richard RM; Rohrdanz MA; Steele RP; Sundstrom EJ; Woodcock HL III; Zimmerman PM; Zuev D; Albrecht B; Alguire E; Austin B; Beran GJO; Bernard YA; Berquist E; Brandhorst K; Bravaya KB; Brown ST; Casanova D; Chang C-M; Chen Y; Chien SH; Closser KD; Crittenden DL; Diedenhofen M; DiStasio RA Jr.; Dop H; Dutoi AD; Edgar RG; Fatehi S; Fusti-Molnar L; Ghysels A; Golubeva-Zadorozhnaya A; Gomes J; Hanson-Heine MWD; Harbach PHP; Hauser AW; Hohenstein EG; Holden ZC; Jagau T-C; Ji H; Kaduk B; Khistyaev K; Kim J; Kim J; King RA; Klunzinger P; Kosenkov D; Kowalczyk T; Krauter CM; Lao KU; Laurent A; Lawler KV; Levchenko SV; Lin CY; Liu F; Livshits E; Lochan RC; Luenser A; Manohar P; Manzer SF; Mao S-P; Mardirossian N; Marenich AV; Maurer SA; Mayhall NJ; Oana CM; Olivares-Amaya R; O'Neill DP; Parkhill JA; Perrine TM; Peverati R; Pieniazek PA; Prociuk A; Rehn DR; Rosta E; Russ NJ; Sergueev N; Sharada SM; Sharmaa S; Small DW; Sodt A; Stein T; Stück D; Su Y-C; Thom AJW; Tsuchimochi T; Vogt L; Vydrov O; Wang T; Watson MA; Wenzel J; White A; Williams CF; Vanovschi V; Yeganeh S; Yost SR; You Z-Q; Zhang IY; Zhang X; Zhou Y; Brooks BR; Chan GKL; Chipman DM; Cramer CJ; Goddard WA III; Gordon MS; Hehre WJ; Klamt A; Schaefer HF III; Schmidt MW; Sherrill CD; Truhlar DG; Warshel A; Xua X; Aspuru-Guzik A; Baer R; Bell AT; Besley NA; Chai J-D; Dreuw A; Dunietz BD; Furlani TR; Gwaltney SR; Hsu C-P; Jung Y; Kong J; Lambrecht DS; Liang W; Ochsenfeld C; Rassolov VA; Slipchenko LV; Subotnik JE; Van Voorhis T; Herbert JM; Krylov AI; Gill PMW; Head-Gordon M Advances in molecular quantum chemistry contained in the Q-Chem 4 program package. Mol. Phys 2015, 113, 184–215.

(64). Legault CY CYLView, version 1.0b; Université de Sherbrooke, 2009. http://www.cylview.org.

(65). Day JI; Weaver JD Selective and Scalable Perfluoroarylation of Nitroalkanes. J. Org. Chem 2017, 82 (13), 6801–6810. [PubMed: 28598158]

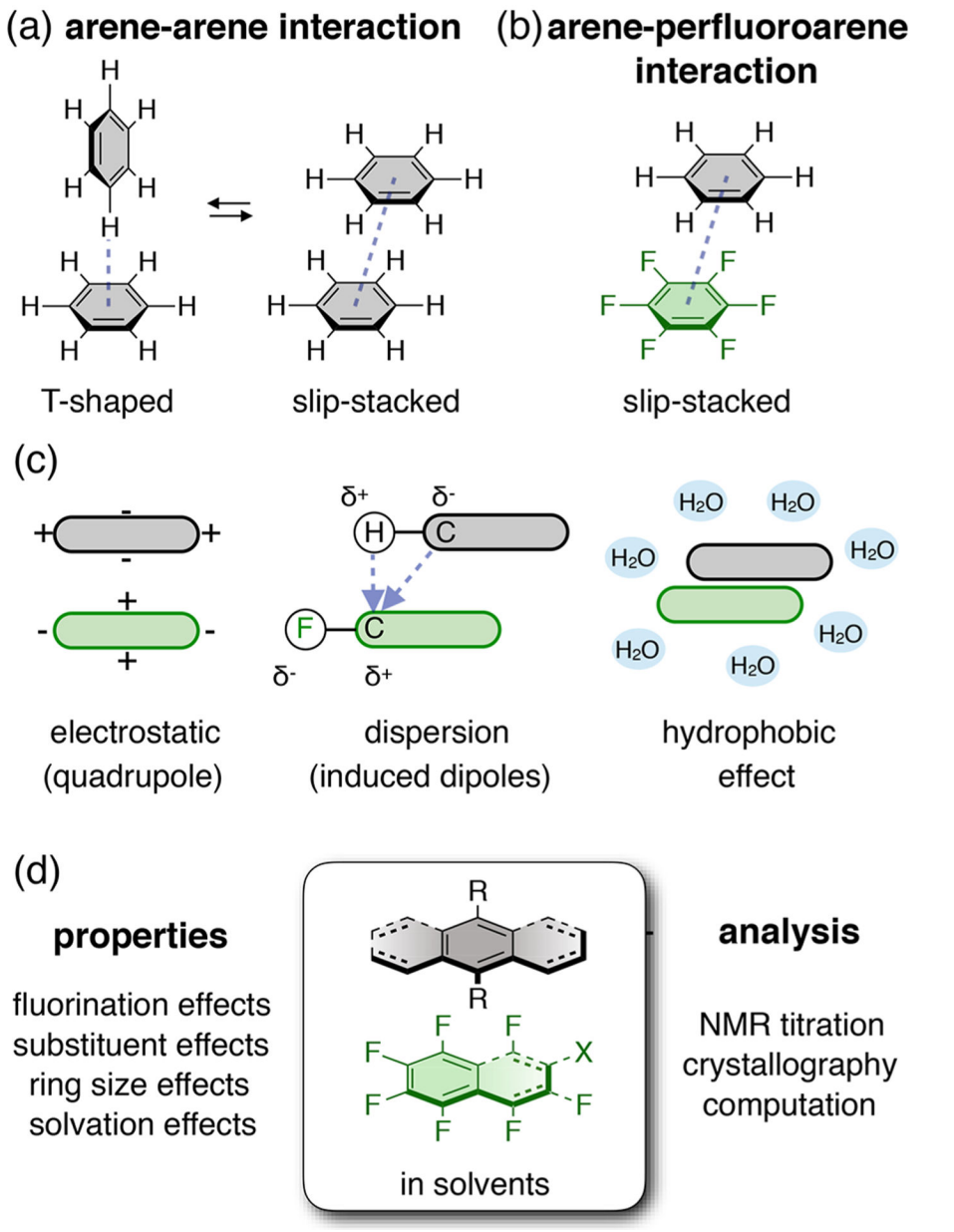

Figure 1.

(a) Ground state geometries of arene-arene interaction. (b) Ground state geometry of benzene-perfluorobenzene interaction. (c) Key stabilizing factors for arene-perfluoroarene interactions in solution. (d) Overview of studies reported herein, focusing on properties that affect arene-perfluoroarene interactions in solution using titration, crystallography, and computation.

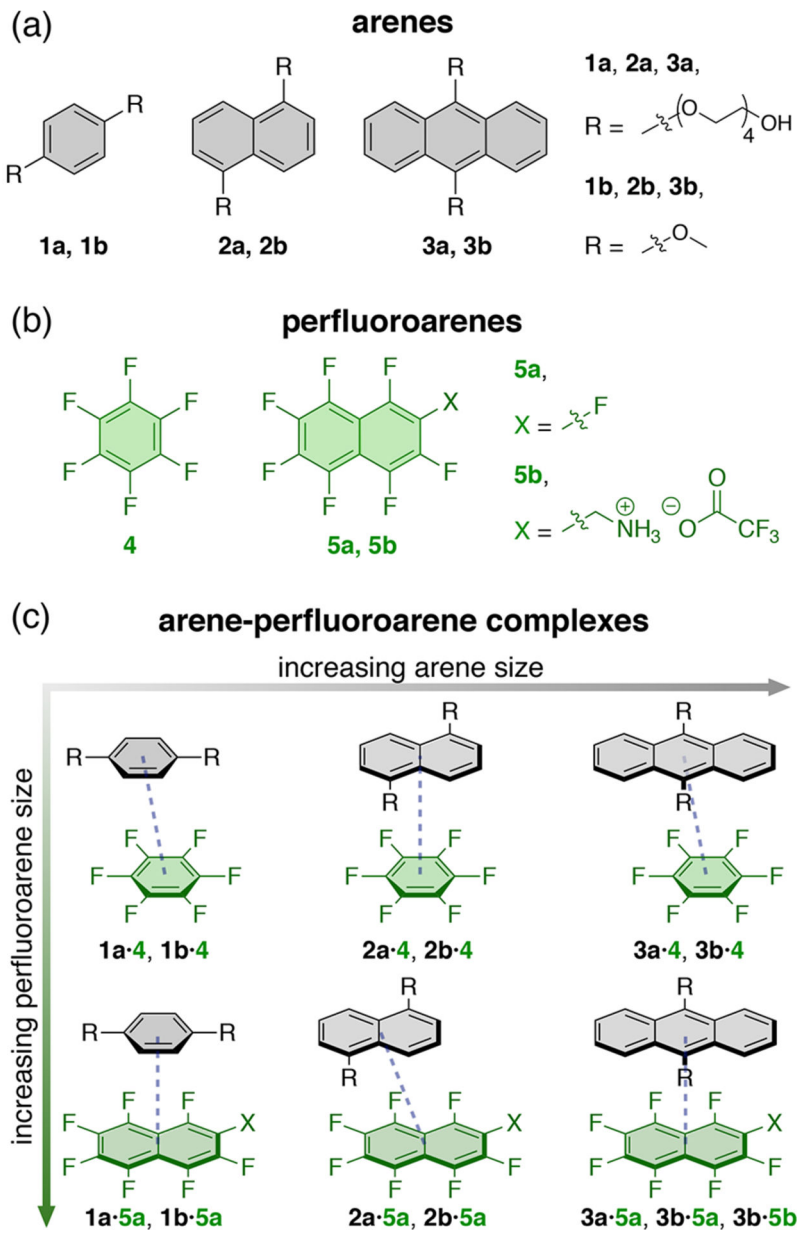

Figure 2.

Arenes (a) and perfluoroarenes (b) for measuring binding affinities in organic and aqueous solution. Arenes **1a**, **2a**, and **3a** were prepared for titration experiments. Arenes **1b**, **2b**, and **3b** were prepared for crystallography. Simple perfluorobenzene (**4**) and perfluoronaphthalene (**5a**) were used in titration experiments in organic solvents. Functionalized perfluoronapthalene **5b** was used in titration experiments in aqueous solvents. (c) Six arene-perfluoroarene complexes of varying sizes employed to study the ring size, fluorination, substituent, and solvation effects in arene-perfluoroarene interactions.

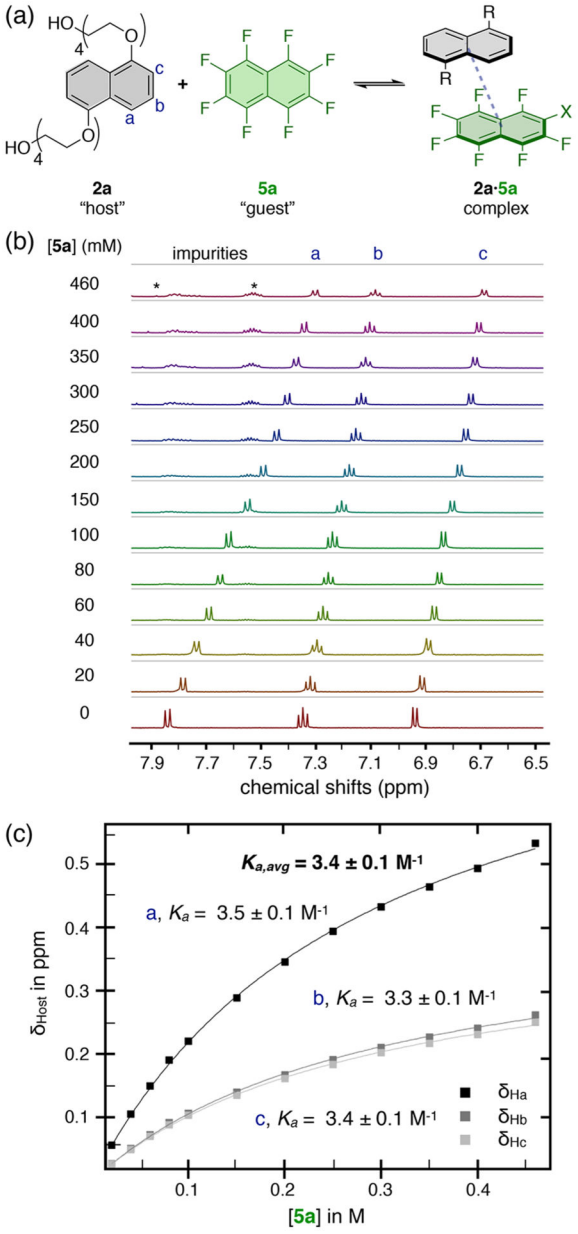

Figure 3.

(a) Representative binding affinity determination experiment using compounds **2a** and **5a**. (b) ^{1}H NMR titration of complex **2a·5a** in CD_3OD. Chemical shifts shown are the aromatic region of arene **2a**. *Octafluoronapthalene impurities. (c) Representative binding isotherm. Arene aromatic signals were monitored and fitted using a 1:1 binding equilibrium equation in IgorPro.

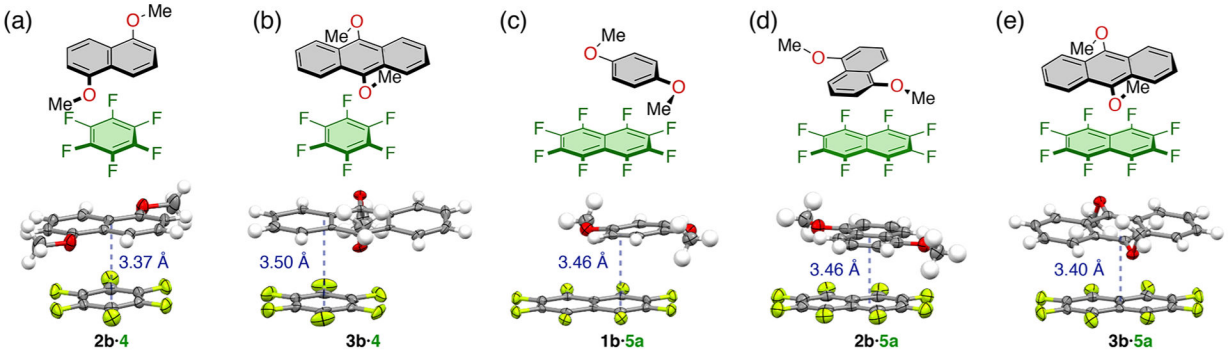

Figure 4.

Crystal structures of arene-perfluoroarene complexes. Ellipsoids are shown at 75% probability level and the principal ellipses are shown with black lines. Cocrystals are obtained by slow evaporation of 1,2-dichloroethane and hexane (for **2b·4** and **3b·4**), 1,2-dichloroethane and diethyl ether (for **1b·5a** and **3b·5a**), and 1,2-dichloroethane and toluene (**2b·5a**) from 1:1 mixtures of arenes and perfluoroarenes at overall 0.2 M concentrations.

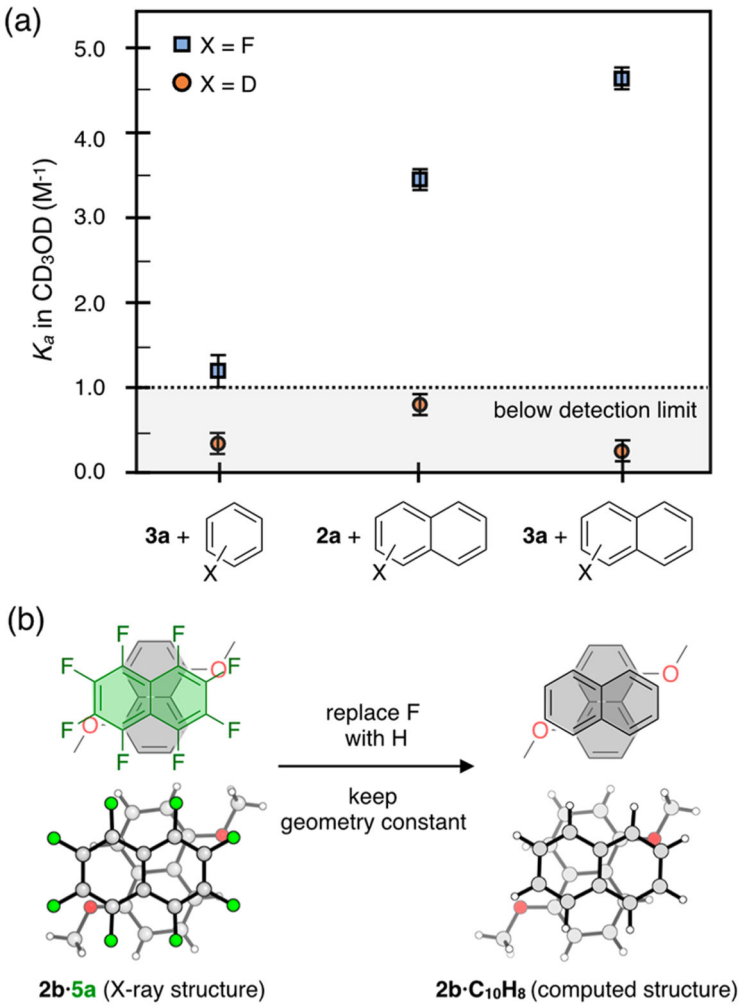

(c)

complex	ΔE_{elec}	ΔE_{disp}	ΔE_{Pauli}	ΔE_{pol}	ΔE_{CT}	ΔE_{int}
2b·5a	-18.3	-18.3	24.8	-1.7	-0.2	-13.8
2b·$C_{10}D_8$	-13.8	-16.7	25.5	-0.8	-0.4	-6.2

Figure 5.

Experimental and computational results of fluorination effects. (a) Experimental comparison of arene-arene (K_a (X = D)) and arene-perfluoroarene (K_a (X = F)) interaction in CD_3OD. Dotted line indicates when K_a = 1 M^{-1} and the gray area indicates NMR detection limit (K_a < 1 M^{-1}). Blue = guest is perfluoroarene. Orange = guest is perdeuteroarene. (b) Methodology of computational analysis of the fluorination effect using truncated **2b·5a**. (c) Energy decomposition analysis (second generation ALMO-EDA) on the cocrystal structure, **2b·5a**, and truncated computed structure, **2b·$C_{10}H_8$**. Total interaction energies and energy breakdowns are calculated using B97M-V and revPBE functionals with the def2-svpd basis set. Energies in kcal mol^{-1}. ΔE_{elec} = electrostatic. ΔE_{disp} = dispersion. ΔE_{Pauli} = Pauli repulsion. ΔE_{pol} = polarization. ΔE_{CT} = charge transfer. ΔE_{int} = total interaction energy.

(a)

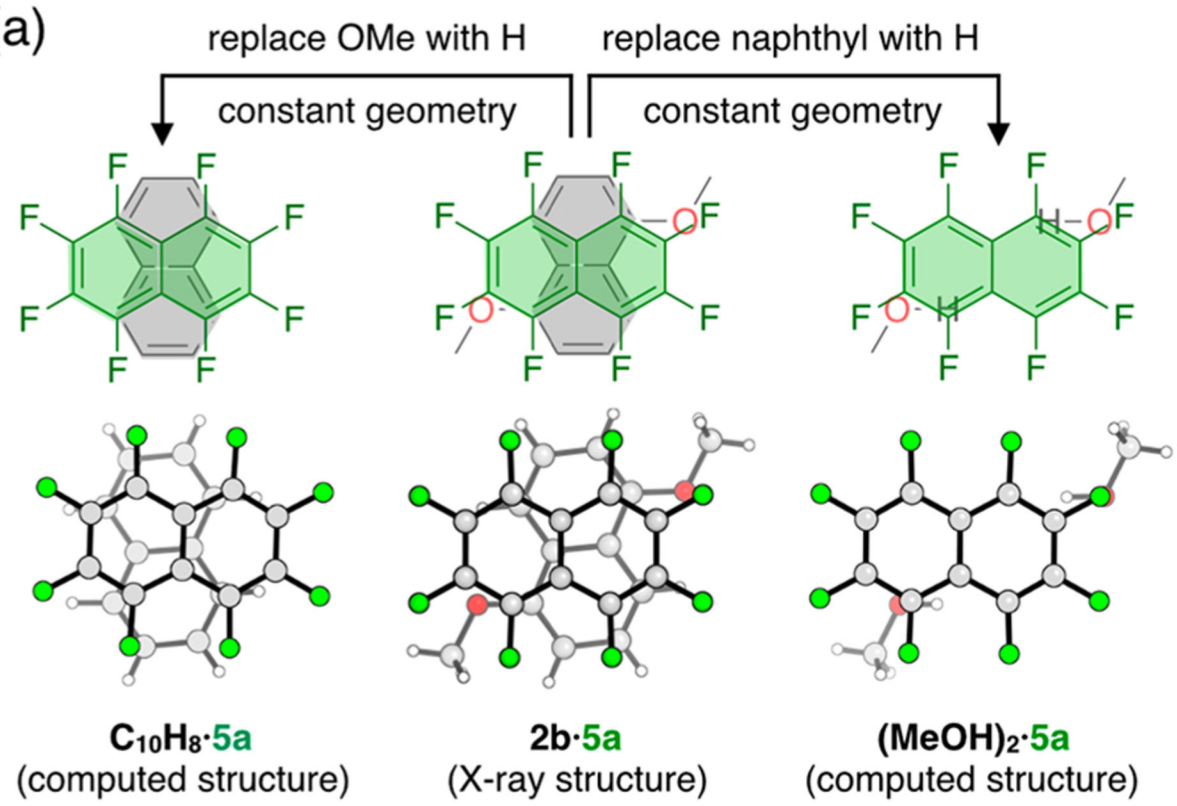

(b)

complex	ΔE_{elec}	ΔE_{disp}	ΔE_{Pauli}	ΔE_{pol}	ΔE_{CT}	ΔE_{int}
2b·5a	-18.3	-18.3	24.8	-1.7	-0.2	-13.8
$C_{10}H_8$·5a	-15.3	-15.6	22.0	-1.3	0.0	-10.2
$(MeOH)_2$·5a	-5.3	-3.9	5.7	-0.5	-0.2	-4.2

Figure 6.

Computational study of substituent effects. (a) Scheme of computational analysis on the substituent effects using truncated **2b·5a**. (b) Energy decomposition analysis (second generation ALMO-EDA) on the cocrystal structure, **2b·5a**, and truncated computed structures, **$C_{10}H_8$·5a** and **$(MeOH)_2$·5a**. Total interaction energies and energy breakdowns are calculated using B97M-V and revPBE functionals with def2-svpd basis set. Energies in kcal mol^{-1}. ΔE_{elec} = electrostatic. ΔE_{disp} = dispersion. ΔE_{Pauli} = Pauli repulsion. ΔE_{pol} = polarization. ΔE_{CT} = charge transfer. ΔE_{int} = total interaction energy.

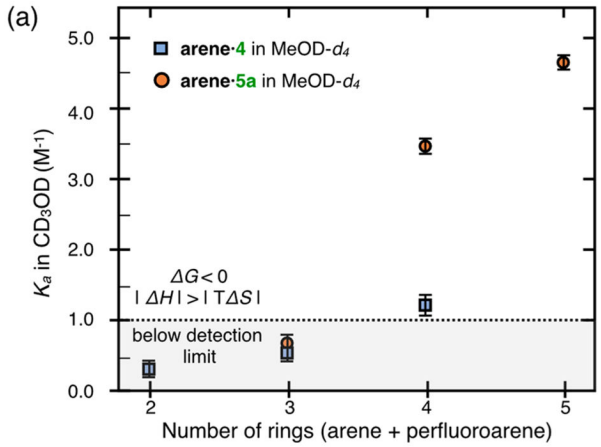

(b)

complex	ΔE_{elec}	ΔE_{disp}	ΔE_{Pauli}	ΔE_{pol}	ΔE_{CT}	ΔE_{int}
2b·4	-16.1	-14.7	21.4	-1.4	-0.1	-10.8
3b·4	-15.3	-14.7	21.1	-1.4	-0.1	-10.4
1b·5a	-15.1	-13.1	19.9	-1.3	-0.3	-9.9
2b·5a	-18.3	-18.3	24.8	-1.7	-0.2	-13.8
3b·5a	-19.9	-20.6	27.8	-1.8	-0.5	-15.0

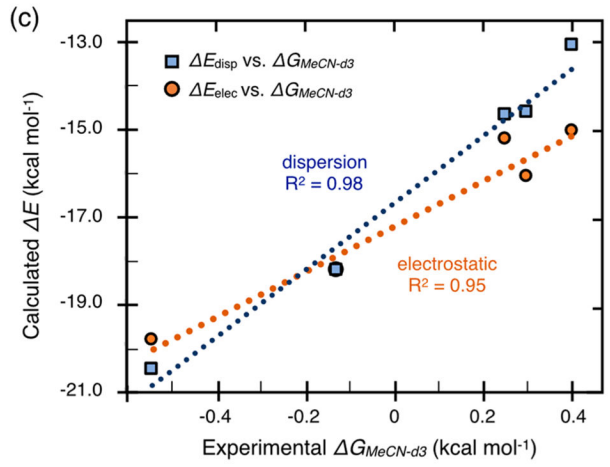

Figure 7.

Experimental and computational study of ring size effects. (a) Experimental K_a measurements of 6 differently sized arene-perfluoroarene complexes in CD_3OD. K_a's are plotted against the number of combined arene and perfluoroarene rings within the arene-perfluoroarene interactions. Dotted line indicates when $K_a = 1\ M^{-1}$ and the gray area indicates NMR detection limit ($K_a < 1\ M^{-1}$). Orange = K_a values for arene·**4** in CD_3OD. Blue = K_a values for arene· **5a** in CD_3OD. (b) Energy decomposition analysis (second generation ALMO-EDA) on the cocrystal structures, **2b·4**, **3b·4**, **1b·5a**, **2b·5a**, and **3b·5a**. (c) Linear free energy relationship (LFER) between calculated ΔE_{disp} or ΔE_{elect} and experimental $\Delta G_{MeCN-d3}$.

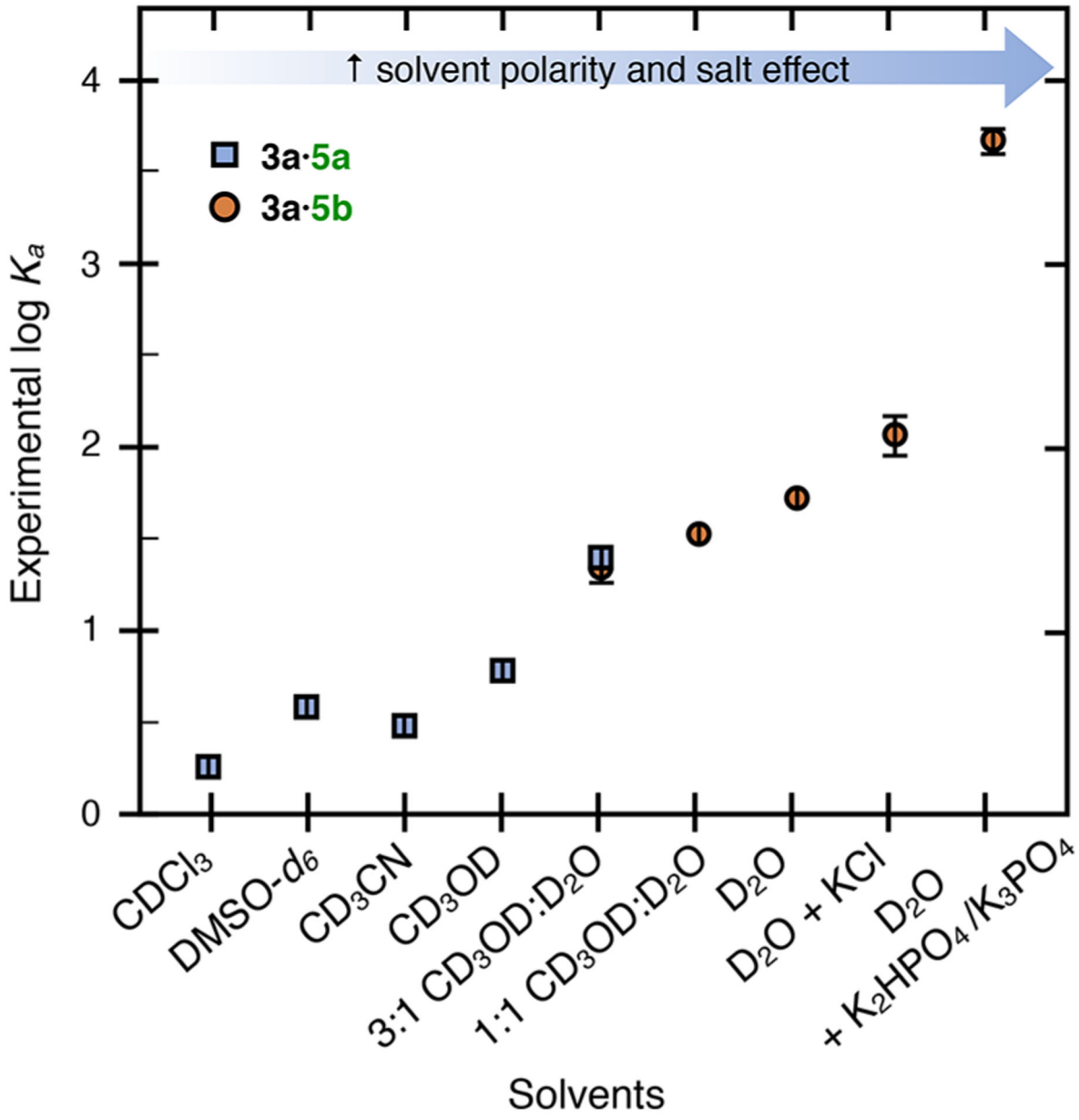

Figure 8.

Experimental study of solvation effects. Graph of K_a with increasing solvent polarity and salt effect. Total salt concentrations were kept at 20 mM.

Table 1.

Summary of Binding Affinity (K_a) Data Obtained from NMR Titrations of Arene-Perfluoroarene, Arene-Arene, and Perfluoroarene-Perfluoroarene Dimers[a]

entry	complex	solvent	K_a (M^{-1})
1	**1a·4**	CD_3CN	<1
2	**1a·4**	CD_3OD	<1
3	**2a·4**	CD_3CN	<1
4	**2a·4**	CD_3OD	<1
5	**3a·4**	$CDCl_3$	<1
6	**3a·4**	CD_3CN	<1
7	**3a·4**	DMSO-d_6	1.1 ± 0.1
8	**3a·4**	CD_3OD	1.2 ± 0.2
9	**3a·4**	3:1 CD_3OD:D_2O	1.4 ± 0.1
10	**1a·5a**	CD_3CN	<1
11	**1a·5a**	CD_3OD	<1
12	**2a·5a**	CD_3CN	1.9 ± 0.9
13	**2a·5a**	CD_3OD	3.5 ± 0.1
14	**3a·5a**	$CDCl_3$	1.3 ± 0.1
15	**3a·5a**	CD_3CN	2.2 ± 0.1
16	**3a·5a**	DMSO-d_6	2.8 ± 0.2
17	**3a·5a**	CD_3OD	4.7 ± 0.1
18	complex =**3a·5a**	3:1 CD_3OD:D_2O	21.8 ± 0.3
19	**3a·5b**	3:1 CD_3OD:D_2O	18.9 ± 0.5
20	**3a·5b**	1:1 CD_3OD:D_2O	30.0 ± 0.5
21	**3a·5b**	D_2O	49 ± 1
22	**3a·5b**	D_2O + KCl	120 ± 50[b]
23	**3a·5b**	D_2O + K_2HPO_4/K_3PO_4	6000 ± 1000[b]
24	**3a·C_6D_6**	CD_3OD	<1
25	**3a·$C_{10}D_8$**	CD_3OD	<1
26	**2a·$C_{10}D_8$**	CD_3OD	<1

[a]All K_a's were obtained in duplicate. Error ranges are determined within 95% confidence interval (see SI).

[b]Only H_a (most downfield shifted aromatic proton) was used, as other aromatic protons gave an overall small shift change (<0.005 ppm).